Article | Received 30 June, 2026; Accepted 20 September, 2026; Published 10 October, 2026
https://doi.org/10.55092/pe20260022

Research on the phase transition phenomena of water vapor in vacuum and cryogenic environments

Yinchao Wang[1], Zihao Yin[1], Zonghao Pan[1], Weiwei Zhang[2,*], Zhezeng Jin[1], Shengyuan Jiang[2]

[1] College of Mechanical and Electrical Engineering, Shenyang Aerospace University, Shenyang, China
[2] State Key Laboratory of Robotics and System, Harbin Institute of Technology, Harbin, China

* Correspondence author; E-mail: zweier@hit.edu.cn.

Abstract: Addressing the technical challenges in in-situ thermal extraction of lunar polar water ice, efficient gas-solid phase transition and collection of water vapor in a vacuum and cryogenic environment hold significant importance. To investigate the gas-solid phase transition of water vapor on cryogenic surfaces under vacuum and extremely low temperatures, this study establishes a simulation of water vapor-gas-solid phase transition in a vacuum cryogenic environment and constructs an experimental setup for water vapor phase transition. The experimental results are compared with the simulation model to analyze the physical mechanisms influencing frost growth under cryogenic conditions. The findings indicate that the solid phase calculated by the simulation model differs in shape and thickness from the experimental results. This is because water vapor releases a large amount of latent heat during the gas-to-solid phase transition, and the low temperatures generated by liquid nitrogen refrigeration are distributed unevenly. Subsequently, based on the physical mechanisms revealed by the experiment, the multi-physics simulation model is corrected. This revised model can simulate the complex morphological phase transition laws of water vapor gas-solid phase transition under vacuum cryogenic conditions, thereby laying a foundation for the efficient collection of water vapor.

Keywords: water vapor; gas-solid phase transition; cryogenic; vacuum

1. Introduction

The introduction gives a concise and appropriate background of the problem under investigation, and the significance, scope and limits of the work. Outline what have done via citing pertinent references. State what your work differs from previous work. Please spell out those highly specialized terms and abbreviations used in the article to make it accessible for readers.

As humanity's deep space exploration progresses into greater depths, the abundant water ice resources within the lunar polar permanently shadowed regions (PSRs) have become a critical material basis for constructing extraterrestrial environmental control and life support systems (ECLSS) and future lunar bases [1]. In recent years, international space missions, exemplified by China's Lunar Exploration Program Phase IV, are accelerating the shift in strategic focus from early remote sensing surveys to in-situ resource utilization (ISRU) of lunar water ice [2,3]. Overcoming the extreme lunar environment to

Copyright©2026 by the authors. Published by ELSP. This work is licensed under Creative Commons Attribution 4.0 International License, which permits unrestricted use, distribution, and reproduction in any medium provided the original work is properly cited.

achieve efficient in-situ extraction and conversion of water resources presents a major technological challenge that urgently needs to be addressed in the field of deep space exploration.

The extreme physical conditions of the lunar surface, characterized by high vacuum and deep cryogenic temperatures, present significant challenges to water ice extraction. Existing research indicates that ice-bearing lunar regolith possesses exceedingly low thermal conductivity and exceptionally high mechanical strength [4]. During in-situ thermal extraction, the sublimated water vapor exists in an extremely rarefied state under the high vacuum environment. Due to the absence of confining atmospheric pressure, the liberated water vapor molecules readily escape into the open vacuum space in a disordered manner. Consequently, the water vapor condensation and collection unit, serving as the critical terminal of the entire thermal extraction system, directly dictates the true acquisition rate of in-situ water resources through its gas-solid phase transition capture efficiency.

In forced convection experiments involving surfaces below −100°C, scholars such as Lee *et al.* observed "bush-like" dendritic ice crystal clusters distinct from those at ambient temperatures, as depicted in Figure 1. They further noted that as the cold wall temperature decreased, the overall frost layer became progressively thinner [5–8].

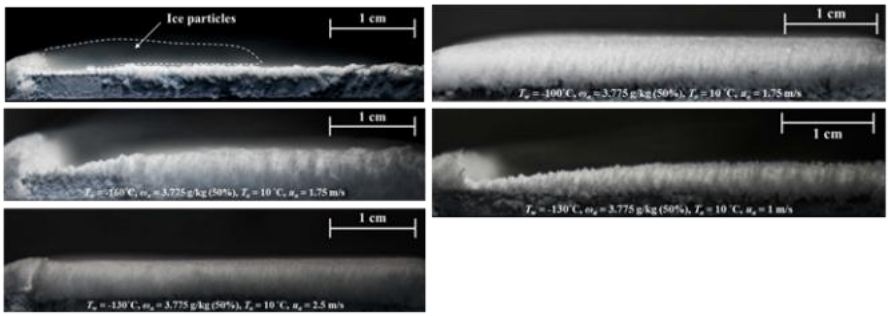


Figure 1. Frost layer growth behavior on cryogenic surfaces under forced convection conditions.

When the extreme condition of vacuum is further superimposed, the phase transition boundary becomes more stringent. In cutting-edge research specific to vacuum cryogenic ice layers, there is a paucity of detailed mechanistic investigations tailored for vacuum cryogenic environments, nor has a robust engineering mapping to the performance optimization of collection device macrostructures been established. To surmount the bottleneck of low collection efficiency in lunar in-situ thermal extraction, this paper systematically investigates the water vapor gas-solid phase transition phenomena within a vacuum cryogenic environment.

2. Gas-Solid Phase Transition Model for Water Vapor in Vacuum Cryogenic Environments

2.1. Water vapor gas-solid phase transition theoretical model

To accurately reflect the dynamic pressure conditions under continuous water vapor collection, this study establishes a 200 Pa environment as the equivalent reference environment for theoretical analysis and numerical modeling. By substituting target operating conditions such as 200 Pa and −100°C into the calculation of the Knudsen number, empirical formulas indicate that the Knudsen number falls within the range of 10 – 4 to 10 – 3. According to the flow regime classification criteria for rarefied gas dynamics (Kn < 0.01), the Knudsen number in the conditions of this study consistently falls within the

continuous medium region, with values ranging from 10^{-4} to 10^{-3}. Therefore, the assumptions of an incompressible Newtonian fluid and a non-slip wall are adopted. The geometric model and boundary conditions are shown in Figure 2.

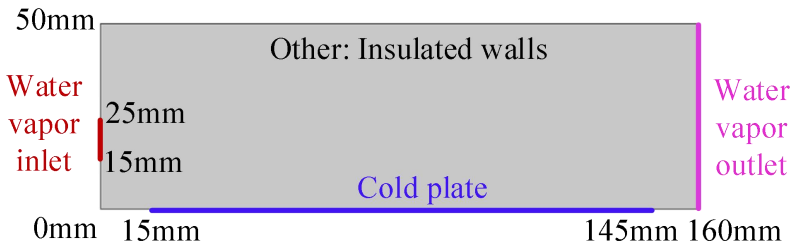


Figure 2. Geometric model and boundary conditions.

In the vacuum and cryogenic environment of the lunar surface, the flow and phase transition of water vapor represent a typical multiphysics problem involving heat and mass transfer. The underlying logic of the simulation is to synchronously solve the control equations for fluid flow, fluid heat transfer, and phase transition using a solver; these physical fields are coupled through state variables.
Therefore, prior to simulation, a theoretical model must first be established.

2.1.1. Laminar flow control equations

The macroscopic flow of water vapor within the model is a prerequisite for heat and mass transfer. Driven by specified inlet velocity and outlet pressure, the airflow within the two-dimensional computational domain is governed by the continuity equation and the incompressible laminar Navier-Stokes equations.

$$\rho\frac{\partial u}{\partial t}+\rho(u\cdot\nabla)u=\nabla\cdot(-pI+\kappa)+F \tag{1}$$

$$\rho\nabla\cdot u=0 \tag{2}$$

In this context, the viscous stress tensor k is defined according to the Newtonian fluid hypothesis as follows:

$$\kappa=\mu\left(\nabla u+(\nabla u)^{}\right) \tag{3}$$

In the momentum conservation control equation for the aforementioned laminar flow, the left-hand side represents the inertial force terms of the fluid microelement, encompassing the transient evolution term and the convective acceleration term; the right-hand side reflects the driving and dissipative mechanisms, including the pressure gradient driving force and the viscous shear dissipation term.
In the multiphysics coupled phase transition model of this study, the volumetric force source term F was defined as a function highly correlated with the solid phase volume fraction, given by:

$$F=-F_{mush}\cdot u=-A_{mush}\cdot\frac{q(1-\theta_l)}{(q+\theta_l)}\cdot u \tag{4}$$

where ρ is the fluid density, kg/m³; κ_σ is the viscous stress tensor, N/m²; μ is the dynamic viscosity of the fluid, $Pa\cdot s$; F is the volumetric force source term acting on the fluid, N/m³; Amush is the phase-

change damping constant, kg/(m3·s); and θ1 is the volumetric fraction of water vapor in the gas phase, dimensionless.

2.1.2. Fluid heat transfer control equations

Sufficient details of the experiment, methods, simulation, calculation, statistical test or analysis should be given so that the method could be repeated by another researcher and the results reproduced. Note and emphasize any hazards such as explosive or toxicity, better with a separate section by the heading "Caution". In theoretical papers, this section can be called "Theoretical Basis" or "Theoretical Calculations".

The heat transfer process is the central link determining whether water vapor can be effectively cooled and trigger phase transition conditions. The cryogenic cold surface generates a strong temperature gradient within the fluid domain, driving efficient heat transfer from the high-temperature mainstream region to the low-temperature cold surface. Under this temperature difference driving force, the thermodynamic energy evolution within the computational domain is dominated by the classical energy conservation equation of convection-conduction.

$$\rho C_p \frac{\partial T}{\partial t} + \rho C_p \mathbf{u} \cdot \nabla T + \nabla \cdot q = Q + Q_p + Q_{vd} \tag{5}$$

Herein, the conductive heat flux q satisfies Fourier's law of heat conduction:

$$q = -k\nabla T \tag{6}$$

q is the heat flux due to conduction, W/m²; k is the thermal conductivity, W/(m·K); Q is the internal volumetric heat source, W/m³; Qp is the heat source term due to work done by pressure, W/m³; Qvd is the heat source term due to viscous dissipation of the fluid, W/m³.

2.1.3. Apparent heat capacity method

Concerning the phenomenon of water vapor directly sublimating to ice near cryogenic cold surfaces in a vacuum environment, this study introduces the apparent heat capacity method to continuously describe the phase transition process. The model treats water vapor (phase 1) and ice (phase 2) as a mixture system, with the governing equations defined as:

$$\rho = \theta_1\rho_1 + \theta_2\rho_2 \tag{7}$$

$$C_p = \frac{1}{\rho}\left(\theta_1\rho_1 C_{p1} + \theta_2\rho_2 C_{p2}\right) + L_{1\to 2}\frac{\partial \alpha_m}{\partial T} \tag{8}$$

$$\alpha_m = \frac{1}{2}\frac{\theta_2\rho_2 - \theta_1\rho_1}{\theta_1\rho_1 + \theta_2\rho_2} \tag{9}$$

Subscripts 1 and 2 denote the gas phase and solid phase, respectively; Cp1 and Cp2 are the specific heat capacities at constant pressure of the two phases, in J/(kg·K); $L_{1\to 2}$ is the latent heat of sublimation of water vapor, in J/kg; α_m is the mass fraction of the phase transition, dimensionless.

Phase transition of water vapor occurs when the local fluid temperature drops below the deposition point. When the volume fraction of gaseous water vapor becomes zero, according to the conservation

condition of volume fraction, the solid-phase volume fraction is considered to be 1. At this point, the local grid cell is macroscopically defined as ice, indicating that a phase transition has occurred.

2.2. Water vapor gas-solid phase transition simulation model

In the initialization and boundary condition setup, the environmental pressure of the chamber was set to 200 Pa, the water vapor temperature was set to 50°C, the cold surface temperature was set to −100°C, and the inlet velocity was set to 0.2 m/s. All other walls where phase transition does not occur were uniformly set as no-slip adiabatic boundaries.

By analyzing the velocity fields, temperature fields, and volume fraction contour plots from COMSOL simulations of gas-solid phase transitions, it is possible to gain a deep understanding of the phase transition mechanisms of water vapor on extremely cold surfaces in a vacuum cryogenic environment.

The simulation results of gas-solid phase transition are presented in Figure 3. A comprehensive analysis of Figure 3 (a) (velocity field contour map), Figure 3 (b) (temperature field cloud map), and Figure 3 (c) (volume fraction map) reveals the following phenomena: upon entering the computational domain through the left inlet of the model, the water vapor flow is constrained by the no-slip boundary condition of the non-phase-transition wall. Driven by laminar flow, the water vapor gradually flows across the cold surface maintained at −100°C. Under the treatment of the apparent heat capacity method, phase transition of water vapor initiates on the cold surface and progresses in a direction perpendicular to the cold surface, leading to a gradual increase in the thickness of the phase-transition layer.

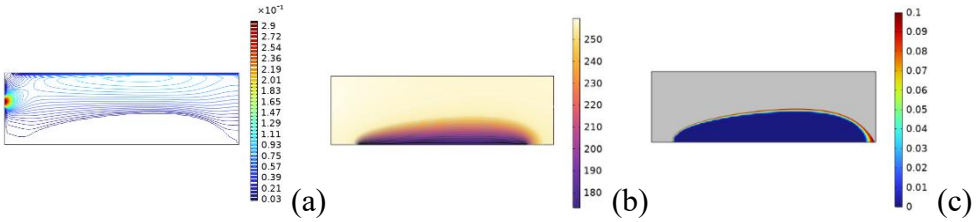


Figure 3. Simulation results of the gas-solid phase transition. **(a)** Velocity field contour plot; **(b)** Temperature field plot; **(c)** Volume fraction plot.

3. Experiments on water vapor phase transitions in a vacuum cryogenic environment and corrections to the simulation mode

3.1. Water vapor phase transition test in a vacuum cryogenic environment

To verify the accuracy of the simulation model's calculation results regarding the gas-solid phase transition of water vapor in a vacuum low-temperature environment, and to examine the actual physical morphology of water vapor following condensation under real working conditions, this study independently developed a test bed for water vapor phase transition in such an environment. The design of the water vapor gas-solid phase transition test bed is illustrated in Figure 4.

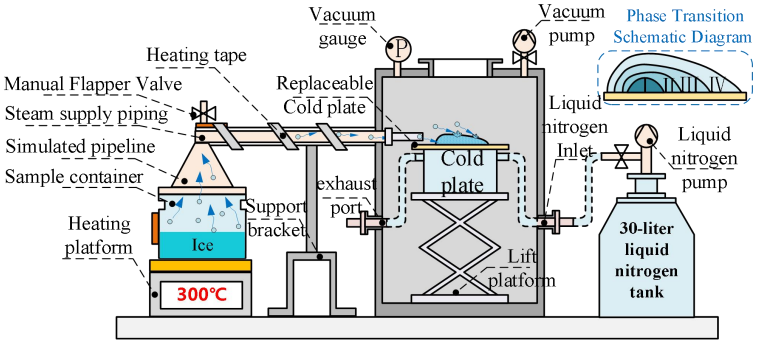


Figure 4. Schematic diagram of the water vapor-solid phase transition test bench.

The physical diagram of the water vapor gas-solid phase change test bench is depicted in Figure 5. The water vapor thermal evaporation unit, which includes a heating table, sample containers, water vapor transport piping, and heating tape, facilitates the heating and evaporation of water samples into water vapor. Located on the right side of the test bench, the vacuum low-temperature environment preparation unit comprises vacuum tanks and liquid nitrogen tanks, which are responsible for creating the vacuum low-temperature environment.

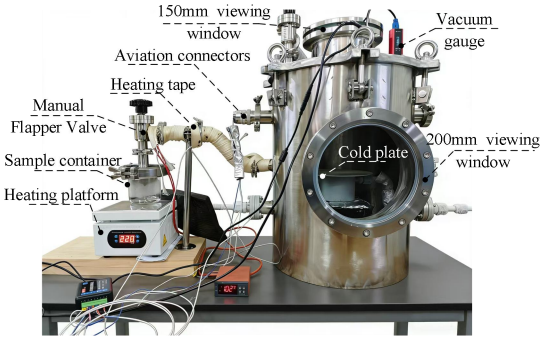


Figure 5. Photograph of the water vapor gas-solid phase change test bench.

3.2. Comparison of experimental results with modified simulation models

The water vapor gas-solid phase change test was performed under conditions of 200 Pa ambient pressure, –100°C cold surface temperature, and 50°C inlet temperature. During the experiment, the phase change of water vapor was observed through the vacuum window on the front side of the vacuum tank and was photographed from an angle parallel to the cold surface to document the phase change process. After 60 minutes, the chilled surface was removed from the cooling stage, and the height of the phase-change solid was measured. The results of the phase-change test are shown in Figure 6.



Figure 6. Results of the water vapor gas-solid phase transition test.

Measurements indicated a solid height of 15 mm after 60 minutes of water vapor phase change. The frost layer resulting from this phase change exhibited significant spatial inhomogeneity. At the front of the condensing wall surface at the channel entrance, water vapor experienced intense condensation, leading to the formation of a thick ice layer characterized by a distinctly raised and rough surface. As the airflow progresses downstream along the cold surface, the thickness of the frost layer decreases sharply, leaving the rear section of the cold surface covered by only a very thin frost film. A comparison between the experimental results and the simulation is presented in Figure 7.

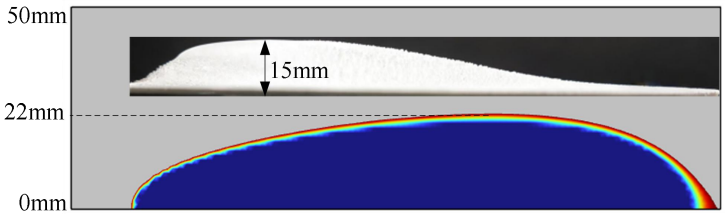


Figure 7. Comparison of experimental and simulated results for the vapor-to-solid phase transition of water vapor.

In response to the comparison between the experimental and simulation results, this study modifies the thermodynamic boundary conditions and momentum control equations of the multiphysics field simulation model. Specifically, the temperature of the originally constant absolute temperature cold surface is rendered non-uniform. To address the left-low-right-high phenomenon observed in the simulation, the volume force damping constant of the phase change volume force is increased within the laminar flow control equation. This adjustment ensures that the resulting thick ice layer adheres to the cold surface, effectively suppressing any unphysical slippage and deformation that may occur in the solid-phase material due to airflow impact. The revised comparison diagrams of the experimental and simulation results are presented in Figure 8.

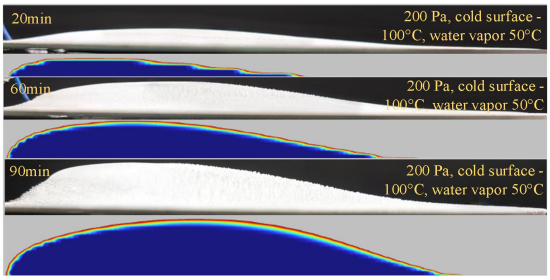


Figure 8. Comparison of the corrected simulation results with experimental data.

4. Analysis of Factors Affecting the Phase Transition of Water Vapor

Utilizing the experimentally validated high-precision multi-physical field coupling model established in the preceding section, this study employs a parametric scanning method to examine the effects of key physical boundary conditions on the water vapor capture efficiency of the cold trap. The research adopts a control variable approach, designating an ambient pressure of 200 Pa, a cold surface temperature of −100 °C, and an inlet flow rate of 0.2 m/s as the baseline control group. Subsequently, the cold surface

temperature, inlet flow rate, ambient pressure, and structural parameters are varied independently to assess the impact of each factor on the distribution characteristics of the resultant solid-phase ice layer.

Under the condition of keeping the flow rate and ambient pressure unchanged, by changing the lowest temperature parameters of the cold surface after the non-uniform temperature treatment (taking −100℃, −90℃, −80℃ respectively), the results of the volume fraction cloud diagrams at the same moment of different temperatures were analyzed, and the results of the volume fraction results of the different temperature parameters are plotted in Figure 9.

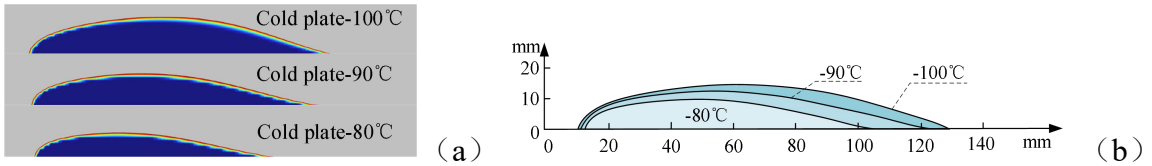


Figure 9. Results of volume fraction at different temperatures. **(a)** Volume fraction at different temperatures; **(b)** Volume fraction distribution at different temperatures.

Under the condition of keeping the flow rate and cold surface temperature unchanged, by changing the ambient pressure parameters (taking 200 Pa, 400 Pa and 600 Pa, respectively), the results of the volume fraction cloud diagrams under different ambient pressures at the same moment were analyzed, and the results of the volume fraction diagrams for different pressure parameters are shown in Figure 10.

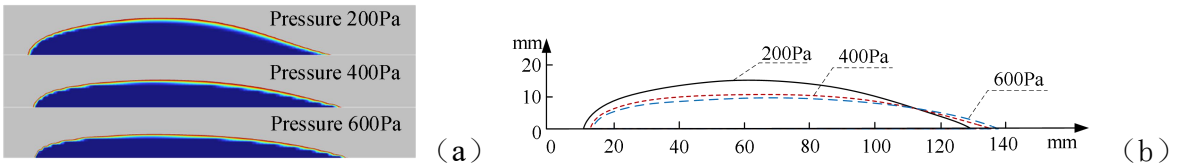


Figure 10. Results of volume fraction as a function of pressure. **(a)** Volume fraction *versus* pressure; **(b)** Volume fraction *versus* particle size.

Under the condition of keeping the ambient pressure and cold surface temperature unchanged, by changing the water vapor flow rate parameters (taking 0.2 m/s, 0.6 m/s and 1 m/s, respectively), the results of the volume fraction cloud maps were analyzed for different flow rates at the same moment, and the resultant maps of the volume fractions for the different flow rate parameters are shown in Figure 11.

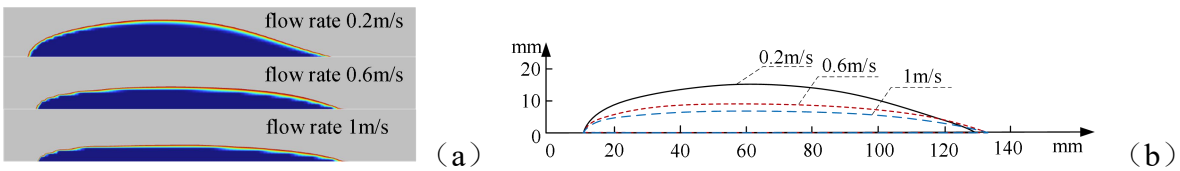


Figure 11. Results of volume fraction for different flow velocity parameters. （**a**）Volume fraction plot for different flow velocities; **(b)** Volume fraction size distribution plot for different flow velocities.

The results of the analysis of the above influencing factors show that, within the parameter range set by the simulation, the efficiency of the gas-solid phase transition is gradually increasing with the decrease of temperature, pressure, and water vapor flow rate, which corresponds to the content of the theoretical model, and verifies the accuracy of the model made. According to the analyzed physical

mechanism, the influence brought by the above factors should be considered comprehensively when the design of water vapor cold trap capture device is carried out subsequently.

5. Conclusion

In this study, a multi-physics coupled simulation model of water vapor gas-solid phase transition is established, and the water vapor gas-solid phase transition experiment is carried out on the basis of the independently constructed gas-solid phase transition experimental platform. The measured ice morphology is compared with the preliminary simulation results, and targeted modifications are made. By comparing the measured ice morphology with the preliminary simulation results and making targeted modifications, the modified simulation was compared with the experiments at different moments with the same physical boundaries, and the morphology and macroscopic dimensions of the water vapor after the phase transition were observed, which further verified the accuracy of the model, and provided a theoretical and simulation basis for the design of the water vapor collection device that needs to be carried out in the following.

Declaration of Generative AI and AI-assisted Technologies

In preparing this manuscript, the author employed generative AI tools exclusively to refine the paper's language, grammar, spelling, and readability. These tools were not utilised to generate the research content, data analysis, experimental results, or academic viewpoints. The research design, experimental procedures, analysis of results, and final content of this paper were all independently completed by the author, who assumes full responsibility for the paper’s integrity, originality, and accuracy.

Acknowledgments

This study was supported by State Key Laboratory of Robotics and Systems (HIT) (SKLRS-2026-KF-15), and the National Major Engineering Key Technology R & D Program, and Basic Scientific Research Business Expense Special Project (Youth Project), No. 20240168.

Authors’ contribution

Conceptualization, Y W; Methodology, Z Y; Data Curation, Z P; Writing-Original Draft, Z Y; Supervision, Y W; Investigation, Z J; Resources, Y W and W Z; Writing-Review & Editing, Y W and S J; Validation. Z P. All authors have read and agreed to the published version of the manuscript.

Conflicts of interests

The authors declare no conflicts of interest. The funders had no role in the design of the study; in the collection, analyses, or interpretation of data; in the writing of the manuscript; or in the decision to publish the results.

Ethical statement

This research did not involve any human or animal experiments.

References

[1] Colaprete A, Schultz P, Heldmann J, Wooden D, Shirley M, *et al.* Detection of water in the LCROSS ejecta plume. *Science*, 2010, 330(6003):463–468.
[2] Zacny K, Luczek K, Paz A, Hedlund M. Planetary volatiles extractor (PVEx) for in situ resource utilization (ISRU), In *Proceedings of the 15th Biennial ASCE Conference on Engineering, Science, Construction, and Operations in Challenging Environments*, Reston, the United States, November 1–3, 2016, pp. 378–390.
[3] Vendiola V, Zacny K, Morrison P, Wang A, Yaggi B, *et al.* Testing of the Planetary Volatiles Extractor (Pvex), In *Proceedings of the 16th Biennial International Conference on Engineering, Science, Construction, and Operations in Challenging Environments*, Reston, the United States, November 15, 2018, pp. 467–480.
[4] Atkinson J, Zacny K. Mechanical properties of icy lunar regolith: Application to ISRU on the moon and mars, In *Mechanical Properties of Icy Lunar Regolith: Application to ISRU on the Moon and Mars*, Reston, the United States, November 15, 2018, pp. 109–120.
[5] Guo Q, Wu Y, Sun J, Li Q, Wei Q. A Review of Research on Frost Formation (In Chinese). *Vacuum*, 2020,57(3):67-72.
[6] Lee J, Lee K.The behavior of frost layer growth under conditions favorable for desublimation. *Int. J. Heat Mass Transf.* 2018, 120:259–266.
[7] Kim C, Lee J, Lee K. Numerical modeling of frost growth and densification on a cold plate using frost formation resistance. *Int. J. Heat Mass Transf.* 2017, 115: 1055-1063.
[8] Jeong H, Byun S, Kim D, Lee K, *et al.* Frost growth mechanism and its behavior under ultra-low temperature conditions[J]. *Int. J. Heat Mass Transf.* 2021, 169: 120941.